Available online at www.sciencedirect.com
ScienceDirect
Sensors and Actuators B 129 (2008) 303–310
SENSORS AND ACTUATORS B CHEMICAL
www.elsevier.com/locate/snb

Surface plasmon resonance sensor based on an array of diffraction gratings for highly parallelized observation of biomolecular interactions

Jakub Dostálek, Jiří Homola *

Institute of Photonics and Electronics, Chaberská 57, 18251 Prague, Czech Republic

Received 12 April 2007; received in revised form 30 July 2007; accepted 5 August 2007
Available online 10 August 2007

Abstract

We report a novel surface plasmon resonance (SPR) sensor for highly parallelized biomolecular interaction analysis (BIA). This sensor utilizes an array detection format and angular spectroscopy of surface plasmons on a two-dimensional array of metallic diffraction gratings. Each diffraction grating on a sensor chip serves both as an SPR coupler and a sensing channel in which refractive index changes induced by biomolecular interaction events are measured. We theoretically optimized the diffraction grating-based sensor to yield maximum resolution in the measurement of refractive index changes. Based on this study, we developed a prototype sensor instrument which enables parallel measurements with high-refractive index resolution (5×10^{-7} RIU) in large number of sensing channels (120). The instrument consists of a two-dimensional array of sensing channels on a sensor chip, a fluidic system for sample delivery, and an SPR optical readout system. By using this instrument and micro spotting to produce a chip array, we evaluated the cross-binding of antibodies against a selected set of endocrine-disrupting compounds (atrazine, 2,4-dichlorophenoxyaceic acid, 4-nonylphenol and benzo[*a*]pyrene) to respective protein–analyte conjugates.

Keywords: Surface plasmon resonance; Surface plasmons; Biosensors; Diffraction grating; High-throughput screening; Biomolecular interaction analysis; Environmental monitoring; Immunoassay

1. Introduction

Surface plasmon resonance (SPR) biosensors have become an established technology for observation of biomolecular interactions [1]. In these devices, binding of biomolecules to their partners anchored on the sensor surface induces an increase in the refractive index (RI) which is probed with a surface plasmon (SP). SPR biosensors offer the advantage of direct detection of biomolecular-binding events without the need of molecular labels. The binding of biomolecules can be monitored in real-time and thus affinity constants can be determined from measured kinetics. Up to now, SPR biosensors were applied for analysis of interactions of numerous biomolecules including proteins [2], oligonucleotides [3,4] and protein–DNA [5].

Nowadays, the majority of SPR biosensors measure RI changes induced by biomolecular-binding events using attenuated total reflection (ATR) method and angular or wavelength spectroscopy of surface plasmons [6,7]. In this approach, variations in the whole SPR spectrum are measured which allows the sensors to achieve a refractive index resolution of $\sim 10^{-7}$ refractive index units (RIU). However, the number of sensing channels provided by spectroscopy of surface plasmon-based instruments is rather limited (<10). In order to enable parallel analysis of biomolecular interactions in a higher number of sensing channels (in the order of hundreds), SPR imaging (SPR microscopy) [8] has been introduced [3,5,9]. SPR imaging systems measure variations in the intensity of light and thus they typically exhibit a considerably lower RI resolution (10^{-5} RIU [10]) compared to the systems based on spectroscopy of surface plasmons. Recently, an SPR imaging with polarization contrast and a special SPR multilayer [11] was demonstrated to improve the RI resolution of SPR imaging technique down to 2×10^{-6} RIU [12].

In this paper, we report an SPR sensor which offers both high-RI resolution and large number of sensing channels. This sensor is based on angular spectroscopy of surface plasmons on a two-dimensional array of metallic diffraction gratings [13]. Through optimization of the operating wavelength, SPR

* Corresponding author.
E-mail address: homola@ure.cas.cz (J. Homola).

0925-4005/$ – see front matter © 2007 Elsevier B.V. All rights reserved.
doi:10.1016/j.snb.2007.08.012

diffraction grating coupler and supporting optical system, we achieved the RI resolution as low as 5×10^{-7} RIU which is comparable with best SPR sensor instruments. The number of sensing channels of 120 provided by the developed SPR sensor instrument significantly exceeds that for conventional spectroscopy of surface plasmon-based SPR sensors. The potential of the developed instrument for highly parallelized biomolecular interaction analysis is demonstrated in an experiment in which we investigated cross-binding of antibodies against a selected set of endocrine-disrupting compounds (atrazine, 2,4-dichlorophenoxyaceic acid, 4-nonylphenol and benzo[*a*]pyrene) using an array of protein conjugates with respective analytes micro-spotted on the sensor chip.

2. Theory

2.1. Diffraction grating SPR coupler

Surface plasmon (SP) is a transverse-magnetic (TM) electromagnetic wave guided along a metal–dielectric interface. SP can be excited with a light wave propagating in the dielectric by means of diffraction on a metallic grating. The coupling between these waves occurs when the components of their propagation constants parallel to the metal surface are matched:

$$k_0 n_b \sin(\theta) + p\frac{2\pi}{\Lambda} = \pm Re\{k_{SP}\}, \quad (1)$$

where k_0 is the propagation constant in vacuum, θ the angle of incidence, n_b the refractive index of the dielectric adjacent to the diffraction grating surface, Λ the modulation period, diffraction order p an integer and k_{SP} is the propagation constant of SP. The coupling of light to SP is manifested as a dip or a peak in the angular or wavelength spectrum of light reflected at the grating surface.

2.2. Geometry of SPR sensor

Let us assume a geometry of diffraction grating-based SPR sensor with angular spectroscopy of SPs depicted in Fig. 1. In this geometry, a monochromatic converging light beam is propagating through an aqueous sample and made incident on a surface of a gold-diffraction grating. On the interface between gold and aqueous sample, the light beam is coupled to SPs through the first diffraction order ($p = 1$) at certain angle of incidence producing a dip in the angular spectrum of reflected light. The angular spectrum is projected on a spatially sensitive detector which allows measuring changes in the angular position of SPR dip $\delta\theta_{SPR}$. Further, we investigate the excitation of surface plasmons on the surface of gold-diffraction grating at the angle of incidence of $\theta_{SPR} = 1.4^\circ$ and at wavelengths between 600 nm and 900 nm.

We used a diffraction grating solver based on the integral method [14] for theoretical investigation of the coupling of a light beam to SPs. Performed simulations presented in Fig. 2a show that the coupling within the selected wavelength range occurs for gratings with the period between 430 nm and 680 nm. As already discussed in Ref. [13], a diffraction grating with sinusoidal modulation enables full coupling of the incident light

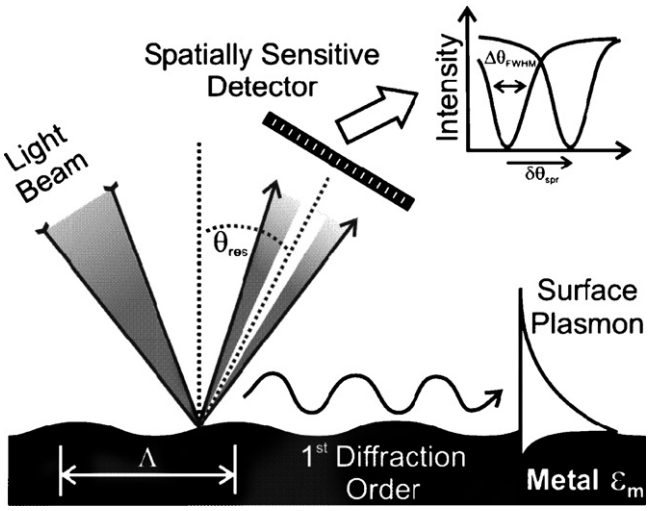

Fig. 1. Scheme of an SPR sensor based on a diffraction grating coupler and angular spectroscopy of SPs.

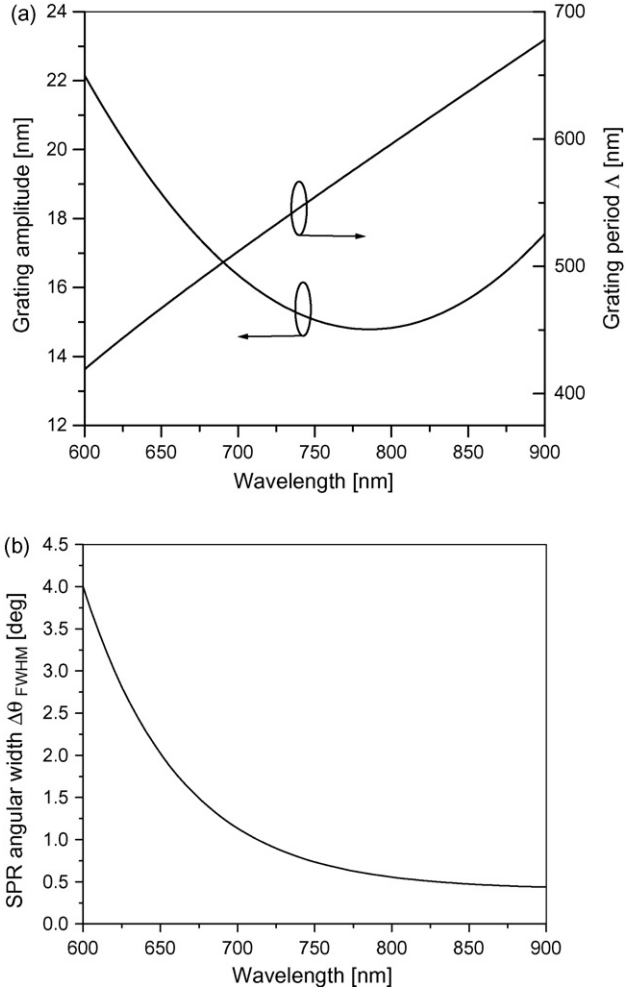

Fig. 2. (a) Wavelength dependence of the amplitude and period Λ of a sinusoidal grating for which full coupling to SP occurs through diffraction at the interface between gold and water; (b) the dependence of full width in half minimum of an SPR dip on the wavelength (angle of incidence close to zero).

beam to SPs at angles of incidence close to zero. Results shown in Fig. 2a reveal that the amplitude of sinusoidal grating providing the full coupling to SPs lies between 14 nm and 22 nm. Using these grating periods and modulation amplitudes of a sinusoidal grating, we determined the wavelength dependence SPR dip width $\Delta\theta_{SPR}$. As shown in Fig. 2b, an order of magnitude lower full width in half minimum is observed at longer wavelengths (e.g., $\Delta\theta_{SPR} = 0.5$ for the wavelength of 900 nm) compared to the shorter wavelengths (e.g., $\Delta\theta_{SPR} = 4^\circ$ for the wavelength of 600 nm).

2.3. Sensitivity to refractive index changing

When the refractive index (RI) of the dielectric adjacent to the sensor surface n_b is changed, the coupling condition to SPs (1) is altered causing a shift in the angular position of SPR dip $\delta\theta_{SPR}$, see Fig. 3a. For small variations in the refractive index, SPR angle shifts linear with δn_b:

$$\delta\theta_{SPR} = S_b \delta n_b, \tag{2}$$

where S_b is the bulk refractive index sensitivity. If a RI change occurs on the metal surface within a thin film with thickness d, much smaller that the penetration depth of surface plasmon $d \ll L_p = 1/[2\, Im\{\sqrt{k_0^2 n_b^2 - k_{SP}^2}\}]$, the induced SPR angle shift can be expressed as

$$\delta\theta_{SPR} = \frac{S_b}{L_p} \delta n_f d, \tag{3}$$

where δn_f is a change in the refractive index of the thin layer. The bulk refractive index sensitivity S_b and the penetration depth L_p depend on a wavelength. From simulations presented in Fig. 3b follow that the bulk sensitivity S_b is higher at shorter wavelengths (e.g., $S_b = 75\ ^\circ\,\mathrm{RIU}^{-1}$ at the wavelength of 600 nm) than at longer wavelengths (e.g., $S_b = 62.5\ ^\circ\,\mathrm{RIU}^{-1}$ at the wavelength of 900 nm). The penetration depth L_p strongly increases with wavelength, for instance $L_p = 62$ and 240 nm at the wavelengths of 600 nm and 900 nm, respectively.

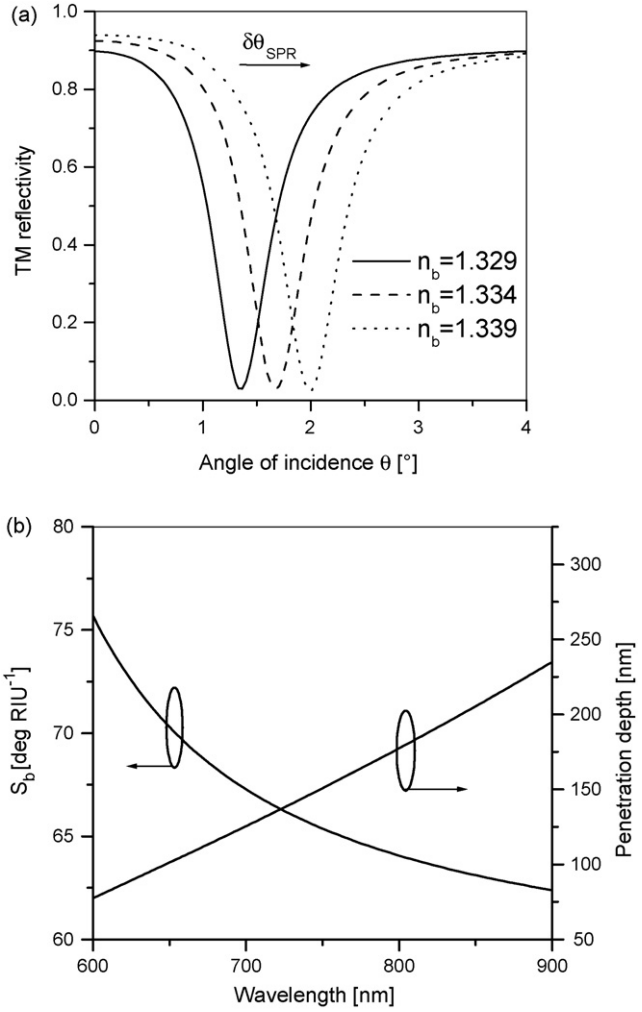

Fig. 3. (a) Angular SPR spectra calculated for the wavelength of 820 nm from gold sinusoidal grating with the amplitude of 15 nm, grating period of $\Lambda = 605$ nm and dielectric with refractive index $n_b = 1.329$ RIU, 1.333 RIU and 1.337 RIU on its top; (b) dependence of the sensitivity S_b and penetration depth L_p on the wavelength (calculated for the parameters in Fig. 2a).

2.4. Optimum operating wavelength of the SPR sensor

The angular position of SPR dip θ_{SPR} can be determined by centroid [15] or polynomial fitting [16] methods applied to the angular reflectivity spectra sequentially acquired from a detector. Assuming the shot-noise is superimposed over the acquired signal from the detector, the standard deviation of the sensor output $\sigma_\theta = \langle[\delta\theta_{SPR} - \langle\delta\theta_{SPR}\rangle]^2\rangle$ is [17]:

$$\sigma_\theta \propto \frac{\Delta\theta_{FWHM}}{\sqrt{N}} = \sqrt{\Delta\theta_{FWHM}\xi}, \tag{4}$$

where N is the number of pixels within the angular width of the SPR dip $\Delta\theta_{FWHM}$ and ζ is the angular spacing of detector pixels. For the angular range mapped on the detector area covering the SPR dip width $\Delta\theta_{FWHM}$ and a certain maximum SPR angle shift $\delta\theta_{SPR} < \Delta\theta_{SPR}^{max}$, the angular spacing ζ can be expressed as

$$\xi \propto \Delta\theta_{FWHM} + \Delta\theta_{SPR}^{max}. \tag{5}$$

As follows from Eqs. (2)–(5), for a maximum angular shift $\Delta\theta_{SPR}^{max}$ induced by a certain surface or bulk refractive index change $\Delta\theta_{SPR,s}^{max} = S_b L_p^{-1} [\delta n_f d]^{max}$ and $\Delta\theta_{SPR,b}^{max} = S_b n_b^{max}$, respectively, the maximum signal to noise ratio of the sensor output can be shown to obey:

$$SNR_s = \frac{\Delta\theta_{SPR,s}^{max}}{\sigma_\theta} \propto \frac{S_b}{L_p\sqrt{\Delta\theta_{FWHM}^2 + \Delta\theta_{FWHM}(S_b/L_p)[\Delta n_f d]^{max}}} = \chi_S, \tag{6}$$

$$SNR_b = \frac{\Delta\theta_{SPR,b}^{max}}{\sigma_\theta} \propto \frac{S_b}{\sqrt{\Delta\theta_{FWHM}^2 + \Delta\theta_{FWHM} S_b \Delta n_b^{max}}} = \chi_B. \tag{7}$$

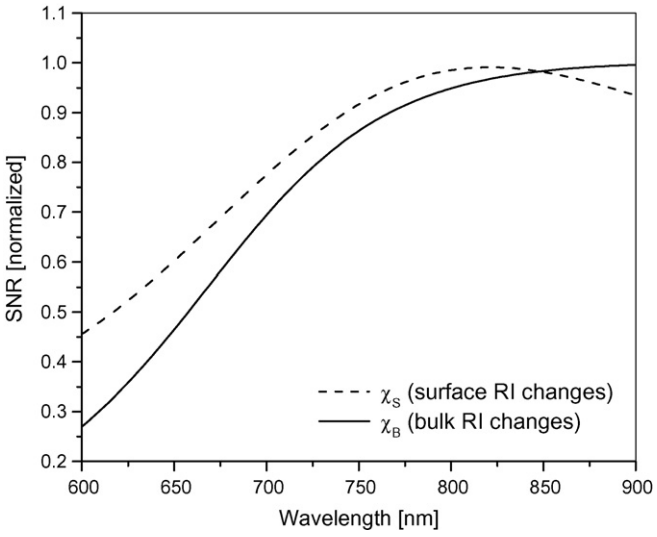

Fig. 4. The dependence of χ_S and χ_B on the wavelength; maximum surface and bulk RI change $[\Delta n_f d]^{max} = 1.7$ nm RIU and $\Delta n_b^{max} = 10^{-2}$ RIU, respectively.

Functions χ_S and χ_B describe the signal to noise ratio of an SPR sensor measuring the surface and bulk RI changes, respectively, regardless of its particular realization. The RI resolution of an SPR sensor is inversely proportional to χ. The operating wavelength providing highest accuracy in the measurement of RI changes can be determined as that for which χ reaches the maximum. Performed simulations presented in Fig. 4b indicate that the optimum operating wavelength for measurement of surface RI changes ($[\Delta n_f d]^{max} = 1.7$ nm RIU) is 820 nm. For measuring of bulk RI smaller than $\Delta n_b^{max} = 10^{-2}$ RIU, the optimum operating wavelength lies close to 900 nm.

3. Experimental

3.1. Materials

C_{11}-chained alkanethiol terminated with di(ethylene glycol) group (C_{11}-chain alkanethiol) was from Prochimia (Poland). C_{16}-mercaptohexadecanoic acid (C_{16}-chain alkanethiol), *N*,*N*,*N*′,*N*′-tetramethyl-*O*-(*N*-succinimidyl)uronium tetrafluoroborate (TSTU) and glutaricdialdehyde were from Sigma–Aldrich (USA). Acetonitrile (ACN), and *N*,*N*′-dimethylformamide (DMF) were from Fluka (Buchs, Switzerland). Monoclonal antibodies (MAb) anti-atrazine a-Atr-D6F3 and a-Atr-E2G2, anti-2,4-dichlorophenoxyacetic acid a-2,4D-E2B5 and anti-nonylphenol a-NP-4H6 were provided by Dr. M. Fránek (Veterinary Research Institute, Brno, Czech Republic) as ascites fluids (antibody represented approximately 10% of protein content). MAb against benzo[*a*]pyrene a-BaP13, purified on the GPC-column, was from Exbio (Prague, Czech Republic). MAb against benzo[*a*]pyrene a-BaP14 was provided by Prof. D. Knopp (Technical University of München, Germany). Conjugates with 4-nonylphenol OV-9pOHPh-non and TG-9pOHPh-non were obtained from Dr. M. Fránek (Veterinary Research Institute, Brno, Czech Republic). The conjugates of bovine serum albumin (BSA) with benzo[*a*]pyrene BSA–BaP-10C2 and BSA–BaP-6C3 were provided by Prof. D. Knopp (Technical University of München, Germany). Conjugates of BSA with atrazine (BSA–Atr) and 2,4-dichlorophenoxyacetic acid (BSA–2,4D) were obtained from Dr. J. Přibyl (National Centre for Biomolecular Research, Masaryk University, Brno, Czech Republic). Bovine serum albumin was purchased from Sigma–Aldrich (USA). All chemicals were used as received without further purification. Deionized water (Millipore apparatus) was used for preparation of all buffers and working media.

3.2. Sensor chip preparation

The sensor chip with the array of gold-diffraction gratings was prepared on the top of a dielectric grating. This grating was prepared from a holographic grating master by soft lithography replication as described previously [13]. The grating parameters were set according to performed theoretical analysis to yield maximum resolution in the measurement of refractive index changes at the sensor surface. The sinusoidal diffraction grating period and amplitude of $\Lambda = 605$ nm and 15 nm, respectively, were used to excite surface plasmons at the wavelength of 820 nm. The replica grating was coated with an adhesion promoting Ti layer (thickness 1.5 nm) and gold layer (thickness 100 nm) by means of electron beam evaporation at the temperature of 150 °C. The evaporation was performed through a mask etched into a phosphor–bronze sheet forming 4 rows of 30 gold-coated gratings providing 120 sensing channels on the sensor chip. The dimensions of each sensing channel were 300 μm × 300 μm and the spacing between the gratings was 500 μm.

The surface of the sensor chip with the array of gold-diffraction gratings was two times cleaned as follows. After 5-min exposure in an ozone cleaner the gold surface was rinsed with deionized water and dried in a stream of pure nitrogen. Then the chip was immersed in the 7:3 mixture of C_{11}-chain and C_{16}-chain alkanethiols dissolved in degassed ethanol (total thiol concentration 1 mM) and stored in a dark place at a room temperature for 2 days to allow the formation of the self-assembled monolayer. Subsequently, the chip was rinsed with ethanol and water and dried in a stream of nitrogen. C_{16}-alkanethiol terminated with a carboxylic head group was used to anchor immunoconjugates while the C_{11}-alkanethiol chain terminated with a diethylene-glycol group formed a stable non-fouling background. The carboxylic terminal groups on the sensor surface were activated with TSTU (1 mg mL^{-1}) dissolved in DMF for 2 h. After the activation, the sensor chip was rinsed with water, dried in a stream of nitrogen and micro-spotted with conjugates. The spotting of different conjugates at different sensing channels was performed by depositing 0.5 μL droplets with conjugates dissolved in phosphate buffer (PB) at the concentration ranging from 1 to 5 mg mL^{-1}. The surface of the sensor chip was coated with BSA to provide a reference and with conjugates BSA–Atr, BSA–2,4D, TG-9pOHPh-non, OV-9pOHPh-non, BSA–BaP-10-C4, BSA–BaP-6C3. After the spotting, the chip was stored at the temperature of 5 °C for 12 h, rinsed with water to wash out unreacted molecules from its surface and dried with a nitrogen stream.

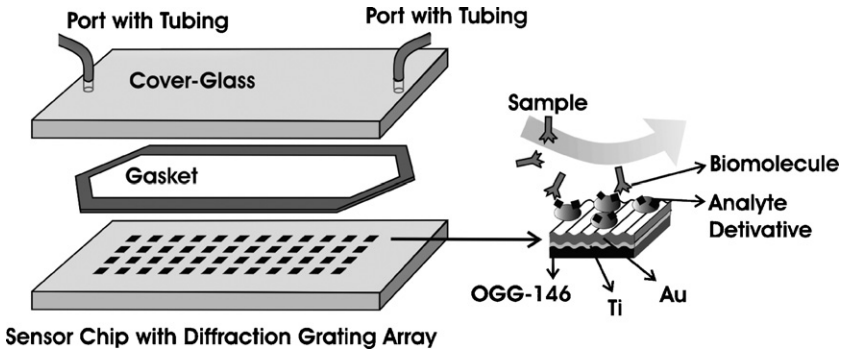

Fig. 5. Scheme of the sensor chip cartridge consisting of the array of diffraction gratings interfaced with the flow-cell consisting of a PDMS gasket and a cover-glass with tubing input and output ports.

3.3. Sensor chip cartridge and SPR optical readout system

As depicted in Fig. 5, the sensor chip with immobilized array of conjugates was mounted in a sensor chip cartridge. In this cartridge, a flow-cell gasket (cast from polydimethylsiloxane [PDMS], the thickness was approximately 100 μm) and a cover-glass (made of polished BK7 glass) were clamped on the sensor chip surface. Input and output ports were drilled into the cover-glass and connected via tubing to a peristaltic pump (Reglo from Ismatec, Switzerland) to flow liquid samples through the sensor cartridge.

The sensor chip cartridge was loaded into the SPR optical readout system in which SPR signal from the array of diffraction gratings was sequentially acquired, see Fig. 6. As a light-source, we used a laser diode (SDL-6502-G1-830-10-G1-.05) connected to a driver (LDX-3525 from ILX Lightwave, USA). The edge-emitting laser diode was temperature stabilized at 13 °C (using temperature controller LTD 5525 from ILX Lightwave, USA) and it emitted diverging light beam at the wavelength 820 nm. The light beam was focused on a rotating diffuser (grade 240 from Optosigma) using a lens, passed through a shutter (VS 14/25 from Uniblitz, USA), polarizer (from Polarcor, USA) and a collimating lens. The collimated light beam was launched into the scanning optics module in which it was focused by a cylindrical lens on a row of 30 sensing channels. The focused light beam was made incident on the sensor chip surface under angles of incidence within the range 0–1.4°. To read all rows of the array, the light beam was scanned across four rows of sensing channels on the sensor chip by using a motorized linear stage (M-111.2DG from PI, Germany). Upon the incidence of the light beam, SPs were excited at certain angle of incidence in each sensing channel producing a dip in the angular distribution of reflected light intensity. The reflected light beam was separated from the incident light by a cube beam-splitter (from Linos, UK) and using imaging optics, the angular reflectivity spectra from an individual row with 30 channels were imaged on a spatially sensitive detector. For detection of angular reflectivity spectra, we used two-dimensional CCD detector DVI 434-FI with 1024 × 1024 pixels and 16 bit AD transducer (from Andor Technologies, Ireland). Using this detector, images were sequentially recorded from four rows of sensing channels and accumulated in time (typically the accumulation of $n_T = 5$ was used for each row). As shown in Fig. 6b, series of bright stripes corresponding to the angular spectra from each diffraction grating within an individual row of sensing channels are visible in the image. In each stripe, a dark band occurs due to excitation of SPs. From each bright stripe, the angular reflectivity spectrum was cut-out and averaged perpendicular to the stripe over n_A

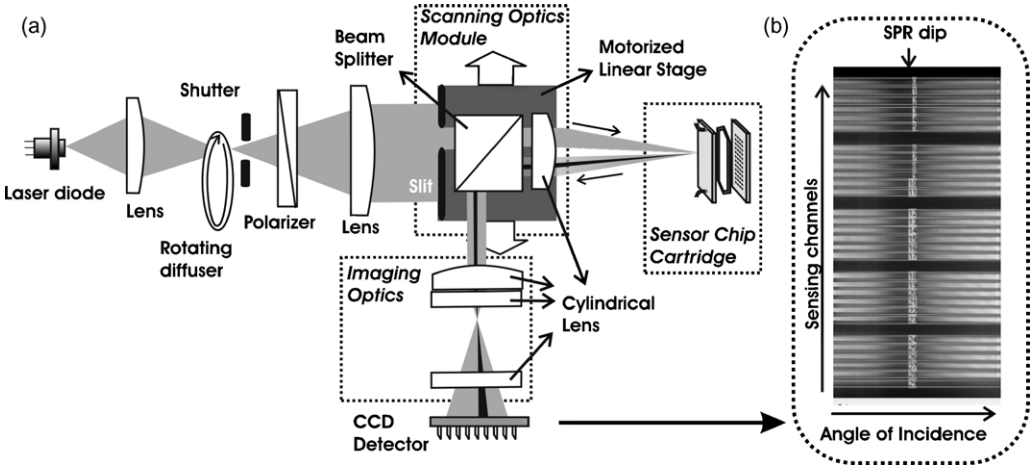

Fig. 6. (a) Optical arrangement of SPR chip reader; (b) typical image with SPR angular reflectivity spectra from an individual row with 30 sensing channels.

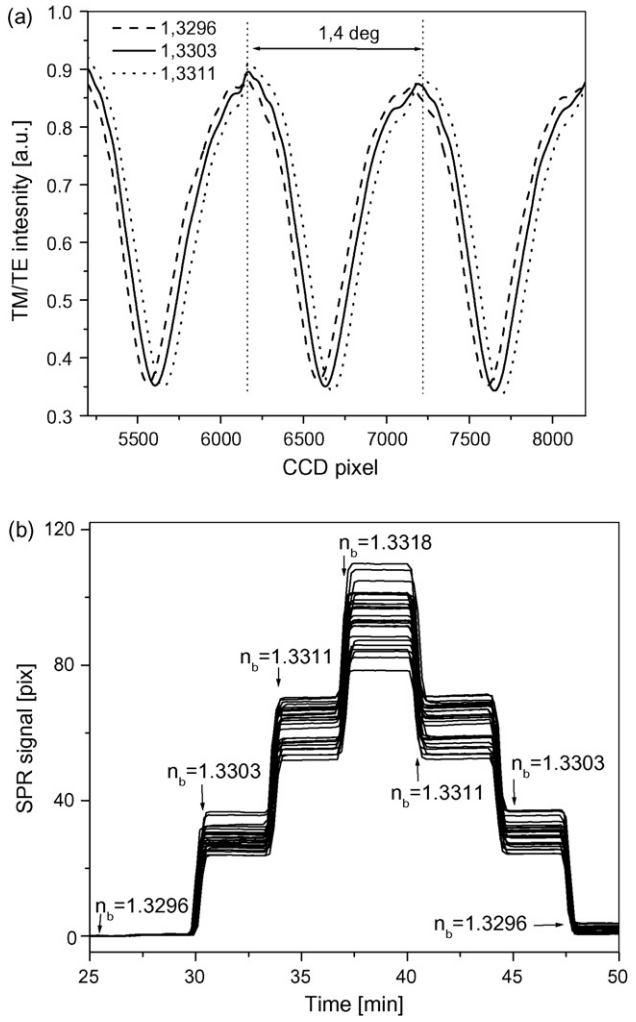

Fig. 7. Refractometric characterization of the SPR sensor: (a) SPR spectra captured for liquids with refractive index 1.3296 RIU, 1.3303 RIU and 1.3311 RIU brought in contact with the sensor surface (three channels shown); (b) time evolution of SPR signal when liquids with refractive index 1.3296, 1.3303, 1.3311 and 1.3318 were sequentially flowed over the sensor surface (30 channels shown).

pixels ($n_A = 10$). From such SPR spectra, the angular position of SPR dip θ_{SPR} was determined in time using a polynomial fitting method. The sensor output was determined as a shift of the SPR angle $\delta\theta_{SPR}$.

3.4. Refractometric characterization

Fig. 7a shows acquired SPR spectrum (compared for three sensing channels) with an SPR dip due to the excitation of SPs. The full width in half minimum of the SPR dip of $\Delta\theta_{FWHM} = 0.6^\circ$ agrees well with that obtained from simulations, see Fig. 2b. As seen in Fig. 7a, the angular position of SPR dip shifts towards higher angles of incidence when the refractive index of a sample flowed through the flow-cell is increased. To determine bulk refractive index sensitivity of the sensor, we sequentially injected liquid samples with refractive indices of $n_b = 1.3296$, 1.3303, 1.3311 and 1.3318 RIU (mixtures of ethylene glycol and water) into the flow-cell and measured the time evolution of the angular position of SPR dip θ_{SPR}, see Fig. 7b. From measured shifts $\delta\theta_{SPR}$ we determined the bulk RI sensitivity of $S_b = 45 \times 10^3$ pixel RIU^{-1} (averaged over sensing channels). As the angular spacing of the detector pixels of $\zeta = 1.37$ millidegree was used, this sensitivity is equal to $S_b = 62^\circ$ RIU^{-1} which is in good agreement with simulations, see Fig. 3b. As seen in Fig. 7b, the measured changes in the sensor signal due to the RI changes varied across the sensing channels due to imperfections of the chip and of the readout system. The standard deviation of bulk RI sensitivity S_b of the whole array of sensing channels was typically below 10%. For the averaging over $n_A = 10$ pixels and accumulation in time of $n_T = 5$, the sensor baseline (signal acquired when a liquid with a constant RI was flowed through the flow-cell) exhibited the standard deviation of 0.026 pixels (averaged over sensing channels) corresponding to $\sigma_\theta = 0.036$ millidegree. This noise superimposed over the sensor output corresponds to the RI resolution σ_θ/S_b of 5×10^{-7} RIU. For these parameters, the readout time from a single row with 30 channels was of 5 s. When the whole array of 4 rows with 120 channels was read, we reduced the accumulation to $n_T = 2$ providing the RI resolution of 8×10^{-7} RIU and the readout time of 15 s.

As illustrated in this section, the main parameters determining the resolution and number of sensing channels of the developed sensor are the averaging time n_A, the accumulation time n_T and the size of the array. These parameters need to be balanced to yield an acceptable array readout time. By using a more sensitive and faster CCD detector and a denser array, both the resolution and number of sensing channels can be potentially further improved.

3.5. Analysis of cross-binding of antibodies to different conjugates

The stock solutions with antibodies a-Atr-D6F3, a-Atr-E2G2, a-2,4-D-E2B5, a-BaP13 and a-BaP14 were dissolved to concentrations 10 μg mL^{-1}, 25 μg mL^{-1}, 5 μg mL^{-1}, 5 μg mL^{-1} and 5 μg mL^{-1}, respectively. The stock solution of antibody a-4-NP-4H6 was diluted at the ratio of 1:10,000. As a-Atr-D6F3, a-Atr-E2G2 and a-2,4-D-E2B5 were used in the form of ascites fluid, the real concentrations of IgG were lower (approximately 10 times) than the given protein content. The binding of antibodies to the array of conjugates was measured in cycles consisting of baseline stabilization, antibody binding, washout and regeneration. The sensor output baseline was established by flowing PB across the sensing surface for 10 min. Then, an antibody was flowed through the flow-cell for 10 min to allow its binding on the protein conjugate array. Subsequently, PB was flowed through the flow-cell for 5 min to wash out loosely bound molecules and regeneration of the sensor was performed using a short (45 s) pulse of 100 mM NaOH containing 10% acetonitrile. The sensor response to binding of an antibody to a conjugate was determined as a change in SPR signal prior to the binding and after the washout. Each SPR signal shift due to binding of an antibody to a conjugate (measured in triplicate) was averaged and reference compensated with the one acquired from channels coated with BSA. The sensor response due to cross-binding of an antibody

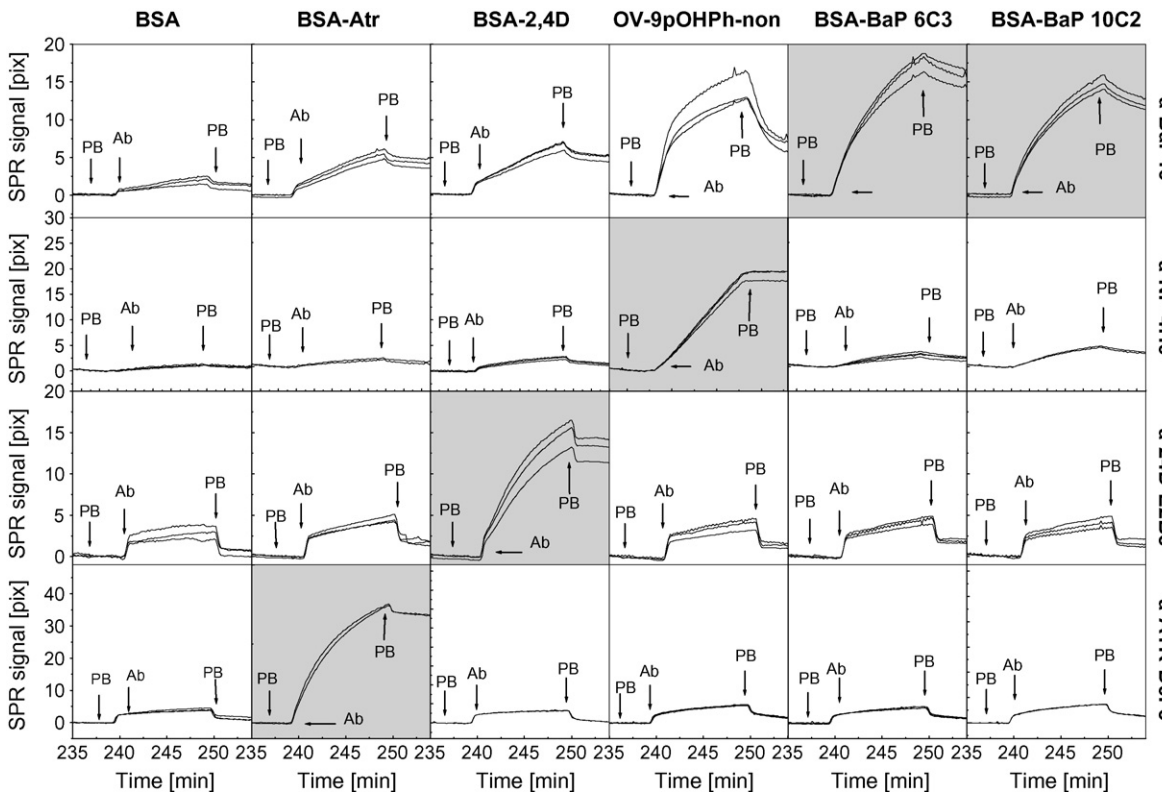

Fig. 8. Sensorgrams measured in triplicates for the binding of antibodies a-Atr-D6F3, a-2,4D-E2B5, a-BaP13 and a-NP-4H6 to sensing channels coated with BSA and conjugates BSA–Atr, BSA–2,4D, OV-9pOHPh-non, BSA–BaP-6C3 and BSA–BaP-10C2. Shaded sensorgrams indicates the specific antibody–conjugate pairs.

to a non-specific conjugate was related to the SPR signal shift measured for the specific conjugate. The variability of the sensor response within the triplicate of identical channels was below 10% (standard deviation).

Solutions with antibodies a-Atr-D6F3, a-Atr-E2B5, a-2,4D-E2B5, a-BaP13, a-BaP14 and a-NP-4H6 were sequentially injected into the sensor with the array of BSA, BSA–Atr, BSA–2,4D, BSA–BaP-6C3, BSA–BaP-10C2, OV-9pOHPh-non and TG-9pOHPh-non. Obtained sensorgrams shown in Fig. 8 reveals that specific binding of a-Atr-D6F3, a-2,4D-E2B5, a-BaP13 and a-NP-4H6 to their respective conjugates BSA–Atr, BSA–2,4D, BSA–BaP-6C3, BSA–BaP-10C2 and OV-9pOHPh-non occurred. The antibody a-Atr-E2B5 and a-BaP-14 did not specifically bind to their respective conjugates and that a-NP-4H6 did not bind specifically to the conjugate TG-9pOHPh-non (not shown in Fig. 8). The cross-binding of a-ATR-D6F3, a-ATR-E2B5 and a-NP-4H6 to non-specific conjugates was lower that 5, 10 and 12%, respectively. The binding of a-BaP antibody to conjugates BSA–BaP-6C3 and 10C2 was of similar level (15.5 and 12.5 pixel, respectively) and it revealed significantly higher cross-binding to BSA–Atr (25%), BSA–2,4D (30%) and OV-9pOHPh-non (41%). This was probably due to a hydrophobic binding pocket of a-BaP giving rise to a non-specific interaction with hydrophobic molecules on the sensor surface (particularly with nonylphenol).

The achieved results reveal specific interaction between the antibodies a-Atr-D6F3, a-2,4D-E2B5, a-BaP13, and a-NP-4H6 and the respective conjugates BSA–Atr, BSA–2,4D, OV-8pOHPh-non, BSA–BaP-6C3 and BSA–BaP-10C2. Using this study, optimum antibodies and conjugate pairs can be selected for a construction of competitive immunoassay for simultaneous detection of atrazine, 2,4-dichlorophenoxyacetic acid, benzo[*a*]pyrene and 4-nonylphenol.

4. Conclusions

In this communication, we report a novel surface plasmon resonance (SPR) sensor instrument for high-throughput biomolecular interaction analysis (BIA). This sensor is based on the angular spectroscopy of surface plasmons on an array of diffraction gratings. Through the optimization of the sensor, a prototype device which offers both highly accurate measurements of refractive index changes induced by binding of biomolecules (RI resolution of 5×10^{-7} RIU) and large number of sensing channels (120) was developed. We demonstrate the potential of this instrument for BIA in the experiment in which we investigated a cross-binding of a set of monoclonal antibodies (against atrazine, 2,4-dichloropenoxyacetic acid, benzo[*a*]pyrene and 4-nonylpenol) to an array of respective conjugates micro-spotted on the sensor chip. In conjunction with technologies enabling the preparation of dense arrays of different molecular probes on the sensor surface, this sensor presents a versatile tool for label-free, high-resolution and highly parallelized observation of biomolecular interactions.

Acknowledgements

The authors would like to thank Dr. Dietmar Knopp (Technical University of Munich) for providing the benzo[*a*]pyrene–BSA conjugate. Dr. Milan Fránek (Veterinary Research Institute, Brno) and Dr. Jan Přibyl (National Centre for Biomolecular Research, Masaryk University, Brno) are gratefully acknowledged for providing several antibodies and other immunoreagents. This work was supported by the European Commission (contract QLK4-CT-2002-02323) and by the Academy of Sciences of the Czech Republic (contract KAN200670701).

References

[1] J. Homola (Ed.), Surface Plasmon Resonance Based Sensors, Springer, 2006.
[2] K.J. Wegner, A.W. Wark, H.J. Lee, E. Codner, T. Saeki, S. Fang, R.M. Corn, Real-time surface plasmon resonance imaging measurement for the multiplexed determination of protein adsorption/desorption kinetics and surface enzymatic reactions on peptide microarray, Anal. Chem. 76 (2004) 5677–5684.
[3] T.T. Goodrich, H.J. Lee, R.M. Corn, Direct detection of genomic DNA by enzymatically amplified SPR imaging measurements of RNA microarrays, J. Am. Chem. Soc. 126 (2004) 4086–4087.
[4] H. Vaisocherová, A. Zítová, M. Lachmanová, J. Štěpánek, Š. Králíková, R. Liboska, D. Rejman, I. Rosenberg, J. Homola, Investigating oligonucleotide interactions at subnanomolar level by surface plasmon resonance biosensor, Biopolymers 82 (2006) 394–398.
[5] J.S. Shumaker-Parry, A. Aebersold, C.T. Campbell, Parallel, quantitative measurement of protein binding to 120-element double-stranded DNA array in real-time using surface plasmon resonance microscopy, Anal. Chem. 76 (2004) 2071–2082.
[6] R. Karlsson, R. Stahlberg, Surface plasmon resonance detection and multispot sensing for direct monitoring of interactions involving low-molecular-weight analytes for determination of low affinities, Anal. Biochem. 228 (1995) 280–284.
[7] J. Dostálek, H. Vaisocherová, J. Homola, Multichannel surface plasmon resonance biosensor with wavelength division multiplexing, Sens. Actuators B 108 (2005) 758–764.
[8] B. Rothenhausler, W. Knoll, Surface-plasmon microscopy, Nature 332 (1988) 615–617.
[9] J.M. Brockman, S.M. Fernandez, Grating-coupled surface plasmon resonance for rapid, label-free, array-based sensing, Am. Lab. 33 (2001) 37–40.
[10] J.S. Shumaker-Parry, C.T. Campbell, Quantitative methods for spatially resolved adsorption/desorption measurements in real time by surface plasmon resonance microscopy, Anal. Chem. 76 (2004) 918–929.
[11] M. Piliarik, H. Vaisocherová, J. Homola, A new surface plasmon resonance sensor for high-throughput screening applications, Biosens. Bioelectron. 20 (2005) 2104–2110.
[12] M. Piliarik, H. Vaisocherová, J. Homola, Towards parallelized surface plasmon resonance sensor platform for sensitive detection of oligonucleotides, Sens. Actuators B 121 (2007) 187–193.
[13] J. Dostálek, M. Miler, J. Homola, Rich information SPR sensor based an array of diffraction gratings, Sens. Actuators B 107 (2005) 154–161.
[14] R. Petit (Ed.), Electromagnetic Theory of Gratings, Springer-Verlag, 1980.
[15] G.G. Nenninger, M. Piliarik, J. Homola, Data analysis for optical sensors based on spectroscopy of surface plasmons, Meas. Sci. Technol. 13 (2002) 2038–2046.
[16] E. Stenberg, B. Persson, H. Roos, C. Urbaniczky, Quantitative determination of surface concentration of protein with surface plasmon resonance using radiolabelled proteins, J. Colloid Interf. Sci. 143 (1991) 513–526.
[17] J. Homola, M. Piliarik, in: J. Homola (Ed.), Surface Plasmon Resonance Based Sensors, Springer, 2006, pp. 45–69.

Biographies

Jakub Dostálek (MS 2000, PhD 2006) was a research assistant at the Institute of Photonics and Electronics in Prague (Czech Republic) from 2000 to 2006 and is currently a postdoctoral fellow at the Max-Planck Institute for Polymer Research in Mainz (Germany). His research interests include guided-wave optics, plasmonics, fluorescence spectroscopy and optical sensors and biosensors. Dr. Dostálek has authored over ten research papers and book chapters.

Jiří Homola (MS 1988, PhD 1993) is head of Photonics Division and chairman of Department of Optical Sensors at the Institute of Photonics and Electronics, Prague (Czech Republic). He also is affiliate associate professor at the University of Washington, Seattle (USA). His research interests are in photonics and biophotonics with emphasis on optical sensors and biosensors. He has edited 2 books and authored 60 research papers in scientific journals and over 120 conference contributions. He is a member of Editorial Board of *Sensors and Actuators B* (Elsevier) and Associate Editor of *Journal of Sensors* (Hindawi).